POLITECNICO DI TORINO
Repository ISTITUZIONALE

All-in-Fiber Electrochemical Sensing

Original
All-in-Fiber Electrochemical Sensing / Richard, I., Schyrr, B., Aiassa, S., Carrara, S., Sorin, F.. - In: ACS APPLIED MATERIALS & INTERFACES. - ISSN 1944-8244. - ELETTRONICO. - 13:36(2021), pp. 43356-43363. [10.1021/acsami.1c11593]

Availability:
This version is available at: 11583/2922252 since: 2021-09-08T20:48:51Z

Publisher:
ACS

Published
DOI:10.1021/acsami.1c11593

Terms of use:

This article is made available under terms and conditions as specified in the corresponding bibliographic description in the repository

Publisher copyright

(Article begins on next page)

19 November 2026

ACS APPLIED MATERIALS & INTERFACES

www.acsami.org

Research Article

All-in-Fiber Electrochemical Sensing

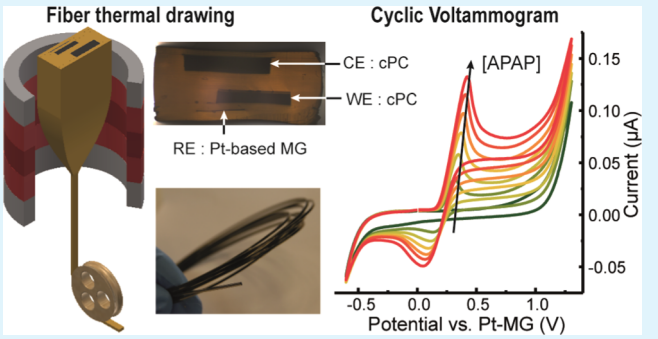
I. Richard, B. Schyrr, S. Aiassa, S. Carrara, and F. Sorin*

Cite This: https://doi.org/10.1021/acsami.1c11593

Read Online

ACCESS | Metrics & More | Article Recommendations | Supporting Information

ABSTRACT: Electrochemical sensors have found a wide range of applications in analytical chemistry thanks to the advent of high-throughput printing technologies. However, these techniques are usually limited to two-dimensional (2D) geometry with relatively large minimal feature sizes. Here, we report on the scalable fabrication of monolithically integrated electrochemical devices with novel and customizable fiber-based architectures. The multimaterial thermal drawing technique is employed to co-process polymer composites and metallic glass into uniform electroactive and pseudoreference electrodes embedded in an insulating polymer cladding fiber. To demonstrate the versatility of the process, we tailor the fiber microstructure to two configurations: a small-footprint fiber tip sensor and a high-surface-area capillary cell. We demonstrate the performance of our devices using cyclic voltammetry and chronoamperometry for the direct detection and quantification of paracetamol, a common anesthetic drug. Finally, we showcase a fully portable pipet-based analyzer using low-power electronics and an "electrochemical pipet tip" for direct sampling and analysis of microliter-range volumes. Our approach paves the way toward novel materials and architectures for efficient electrochemical sensing to be deployed in existing and novel personal care and surgical configurations.



KEYWORDS: *thermal drawing, multimaterial fibers, electrochemical sensors, fiber technology, metallic glasses*

Downloaded via 176.62.155.162 on September 8, 2021 at 18:33:45 (UTC).
See https://pubs.acs.org/sharingguidelines for options on how to legitimately share published articles.

INTRODUCTION

Electrochemical sensors have been widely adopted in analytical chemistry thanks to their sensitivity, experimental simplicity, and low cost. Additive manufacturing methods such as screen printing and inkjet printing technologies have provided a cheap and reproducible method for the mass production of disposable electrochemical devices with consistent chemical performance that are now marketed for industrial, pharmaceutical, or environmental analyses.[1,2] Improvements in conductivity or electroanalytical performances have further been achieved through postprocessing techniques, such as sintering/curing, and surface modification of carbon paste electrode with nanomaterials such as gold nanoparticles,[3] carbon nanotubes,[4] carbon black,[5] and graphene.[6] However, printing technologies require a precise control over the composition and viscosity of conductive inks to guarantee reproducible sensors performances, while being restrained to planar geometries of relatively large dimensions.

Extensive research has been carried out in terms of new electrode configurations and materials to further improve the versatility and sensitivity of electrochemical sensor devices. Micrometer-scale electrodes, for instance, can exhibit attractive features such as improved signal-to-noise-ratio, immunity to ohmic drop, and high mass transport.[7] Recent progresses in this direction include the development of nanoscale pipet-based electrochemical probes as miniaturized tools that can sense and manipulate their environment down to the single-cell level.[8,9] The electrospinning method is also a promising field of research for the production of carbon nanofiber mat electrodes with high surface area, fast electron transfer, and ease of surface functionalization.[10,11] New electrode configurations have also been pursued by means of thee-dimensional (3D) printing technologies for the fabrication of electrochemical sensors at minimal costs, providing ease of fabrication, high batch-to-batch reproducibility, and design flexibility.[12,13] Plastic conductive filaments for electrode printing are, however, currently limited to carbon nanotubes or graphene-infused polymers. As a consequence, most applications require the use of external Ag/AgCl reference and/or platinum counter electrodes, although some works make use of graphite pseudoreference.[12,14,15] Metal-based electrodes have been developed using 3D printing methods,[16,17] but require expensive equipment, an additional electroplating step, and offer a limited electrochemical potential window.[18] Overall, the assembly of both electroactive and reference electrodes in a precise, nonplanar, and scalable way remains a multimaterial processing challenge.

Received: June 21, 2021
Accepted: August 12, 2021

© XXXX The Authors. Published by American Chemical Society

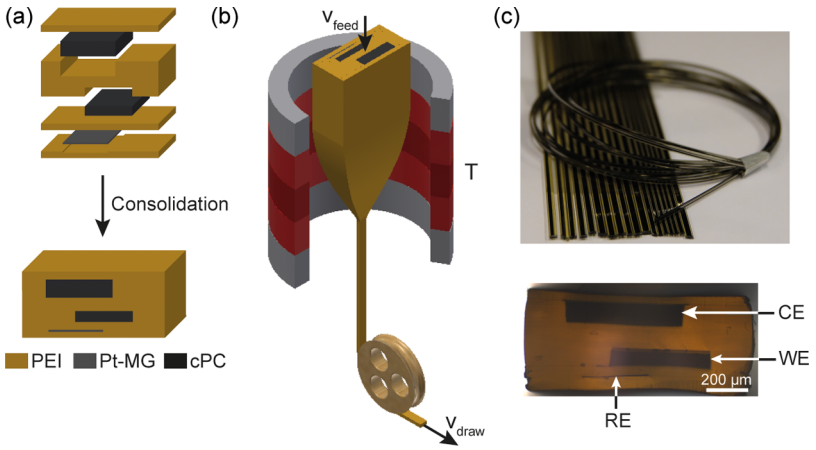


Figure 1. Design and fabrication of electrochemical sensing fibers and capillaries. (a) Illustration of the preform-making process. (b) Illustration of the thermal drawing process for the fabrication of multimaterial and multielectrode fibers. (c) Photograph of drawn fibers and optical micrograph of the fiber cross section.

Functional fibers represent an attractive approach toward integrated electrochemical sensors with novel form factors. Manufacturing by thermal drawing is particularly suited because it allows the simultaneous processing of a variety of conducting and insulating materials into fibers of complex architectures and at a large scale.[19,20] Examples include superelastic fibers based on carbon black-loaded polyethylene[21,22] or liquid metals[23,24] for flexible electronics, structured nanoscale metallic glass fibers for neural stimulation and recording,[25] and carbon nanofiber composites microelectrodes.[26] In particular, carbon black (CB) composites are promising candidates for use as electroactive materials. Indeed, CB-modified electrodes have been widely studied as efficient amperometric sensors, demonstrating competitive electrochemical performances in comparison with carbon nanotube-modified electrodes.[27,28] Furthermore, CB-filled polycarbonate is highly suitable for the fabrication of complex fiber geometries by thermal drawing.[29] In parallel, the ability to draw bulk metallic glasses (BMGs) within polymer fibers and to reach extremely small electrode dimensions and precise arrangements has been recently demonstrated.[25] The amorphous structure of BMGs, free of grain boundaries and crystalline defects, strongly enhance their corrosion resistance.[30−32] The latter combined with their high conductivity make them the ideal candidates to serve as a pseudoreference electrode. In particular, $Pt_{57.5}Cu_{14.7}Ni_{5.3}P_{22.5}$ (Pt-MG)[33] has shown high durability and electrocatalytic activity in fuel cells,[34−36] as well as good biocompatibility.[37]

Here, we report on the scalable fabrication of unified three-electrode electrochemical sensors in an all-in-fiber architecture using the multimaterial thermal drawing approach. The fiber device consists of polymer composite and metallic glass electrodes arranged in a polymeric cladding to form an electrochemical cell with integrated electroactive and pseudoreference functionalities. We demonstrate the versatility of our approach through the fabrication of two original and complementary designs: a fiber tip microelectrode and a high-aspect-ratio fiber-based electrochemical capillary cell. In the microelectrode design, we implement a simple chemical activation step to greatly improve the electroactive performances of CB-filled polymeric electrodes. As a proof of concept, we characterize their behavior for the direct measurement of the common anesthetic drug paracetamol by cyclic voltammetry (CV) or chronoamperometry (CA) and show electron-transfer rates comparable with 3D-printed graphene electrodes as well as superior sensitivity per surface area compared to commercial screen-printed electrodes (SPE). In a second step, we take advantage of a high-surface-area capillary shape to maximize the sensitivity of our electrochemical sensor. The fiber device comprises a hollow core with exposed composite and MG electrodes, and is mounted on top of a conventional laboratory pipet tip, which allows facile sampling of microliter-range volumes and their direct analysis by cyclic voltammetry. We then discuss the effect of inhomogeneities and potential drop in the context of thin polymeric electrodes, the ensuing limitations for the proposed design, and how to alleviate them. Finally, a fully portable system including dedicated low-power electronics is presented, answering the current need for on-site measurements with minimal footprint.

EXPERIMENTAL METHODS

Materials. Polyetherimide plates and conductive polycarbonate (cPC) films were purchased from Boedeker and Goodfellow, respectively. The $Pt_{57.5}Cu_{14.7}Ni_{5.3}P_{22.5}$ master alloys were purchased from PXGroup (Switzerland). Ribbons were prepared by melt spinning on a Cu wheel with a rim speed of 20 m/s. Dimethylformamide (DMF), APAP (*N*-acetyl-*para*-aminophenol, also commonly named acetaminophen, or paracetamol), and phosphate-buffered saline (PBS solution, 10×, pH: 7.4, 10 mM) were purchased from Sigma-Aldrich (Switzerland). A 30 mM stock solution was prepared by dissolving 4.53 mg of APAP in 1 mL of PBS.

Preform Fabrication and Thermal Drawing. The fabrication of the preform is illustrated in Figure 1a. Grooves of proper dimensions were milled inside PEI plates to encase the cPC parts. The latter were obtained by hot pressing cPC films at 180 °C for 20 min under vacuum (Lauffer Pressen UVL 5.0). The complete preforms were consolidated at 240 °C for 30 min in a Meyer Press (Maschinenfabrik Herbert Meyer GmbH). The two preforms were drawn at set temperatures of top: 210 °C, middle: 340 ± 3 °C, bottom: 130 °C, with a feeding speed of 1 mm/min and drawing speeds between 100 and 500 mm/min for the fiber tip and between 100 and 250 mm/min for the hollow fiber.

Structural Characterization. The cross-sectional images of the fibers were taken by light microscopy (Leica DM 2700M). Micrographs of the composite electrodes at the fiber tip were taken using a Zeiss Merlin field emission scanning electron microscope (FESEM) (Zeiss, Göttingen) equipped with a GEMINI II column.

Fiber Probe Preparation. Few centimeter-long probes were cut from the thermally drawn fiber spool using a razor blade. Electrical

https://doi.org/10.1021/acsami.1c11593
ACS Appl. Mater. Interfaces XXXX, XXX, XXX−XXX

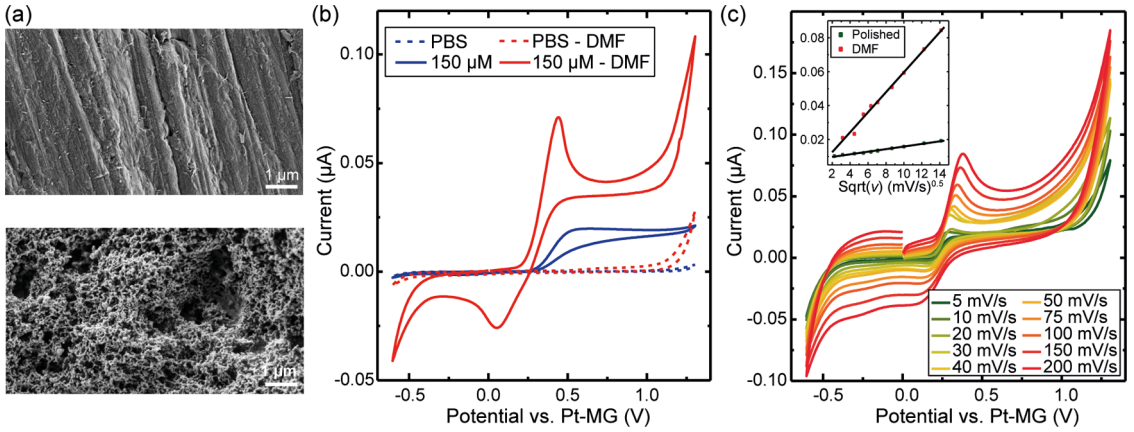


Figure 2. Characterization of WE performance. (a) Electron micrographs of carbon-based composite electrode surfaces after polishing and after chemical treatment, showing the improvement on matrix roughness after dissolution of the polymer matrix with DMF. (b) Cyclic voltammograms showing the influence of chemical treatment on the carbon-based WE response to 150 μM APAP in PBS. The polymer matrix was partially removed by treatment in DMF to improve the active surface area. (c) Cyclic voltammograms of the DMF-treated fiber tip in 100 μM APAP with increasing scan rate from 5 to 200 mV/s. Inset: plot of the peak current vs square root of the scan rate for the polished and DMF-treated fiber tip.

connections were achieved by milling the cladding material to expose the electrodes and connect them with conductive wires. Silver paint was added to ensure a low-resistance contact and the connections were protected with a bicomponent epoxy resin to increase their mechanical resistance. The fiber tip was polished with sandpapers (2000 grit followed by 4000 grit) wetted with distilled water to obtain debris-free, flat, and homogeneous surface. The cPC surfaces were chemically activated by dipping the fiber for 10 s in acetone, followed by drying for 5 min in vacuum at 80 °C, and finally dipping for 10 s in DMF to partially dissolve the insulating polycarbonate matrix.

Electrochemical Characterization. Electrochemical measurements were performed using an Autolab potentiostat (PGSTAT128N, Metrohm). The experiments were carried out at room temperature in PBS as an electrolyte. The OCP measurements were performed in a two-electrode configuration using a fiber with exposed Pt-MG as the working electrode and an Ag/AgCl reference electrode (K0265 AMETEK). Cyclic voltammograms were acquired using the three in-fiber electrodes (Pt-MG as the reference electrode (RE), cPC as the working electrode (WE) and counter electrode (CE)). APAP was added to the electrolyte at the desired concentration, and the solution was stirred for 1.5 min at 250 rpm before recording the voltammogram. Three voltammograms were recorded at a scan rate of 50 mV/s between voltages of −0.6 and 1.3 V and the third voltammogram was used for calibration. The chronoamperometric response was measured with the same set-up under a potential of 500 mV and a constant stirring of 100 rpm. For the electrochemical capillary cell, 20 μL of solution was drawn in the hollow core fibers before each test and the CV measurements were carried out at a scan rate of 20 mV/s. All of the fiber probes were washed with distilled water between the different tests. The heterogeneous rate constant k_0 was estimated by performing cyclic voltammograms at different scan rates and following the procedure proposed by Klingler and Kochi[38,39] for electrochemically irreversible systems using eq 1

$$k_0 = 2.18\left(\frac{D\beta nF\nu}{RT}\right)^{1/2}\exp\left(-\frac{\beta^2 nF}{RT}\Delta E_p\right) \quad (1)$$

where D is the diffusion coefficient of APAP (6.6×10^{-6} cm^2/s[40]), β is the transfer coefficient (assumed 0.5), n is the number of electrons transferred ($n = 2$), F is the Faraday constant, ν is the scan rate, R is the gas constant, T is the temperature, and ΔE_p is the peak-to-peak distance.

RESULTS AND DISCUSSION

The process begins with the fabrication of a macroscopic preform housing the different conductive materials arranged within a supportive cladding. Based on the list of drawable materials (Table S1), we identified carbon black-filled polycarbonate (cPC), a PtCuNiP-based metallic glass, and polyetherimide as materials with reciprocal thermomechanical compatibility during thermal drawing. Carbon black composites combine a high electrical conductivity and high electrochemical inertia, and are low-cost alternatives to carbon nanotubes or graphene.[41]

The stability of Pt-MG electrode in a PBS has been demonstrated for cyclic voltammetry in a previous work and it is confirmed by a stable open-circuit potential (OCP) as shown in Figure S1.[25] The preform is processed by simple machining techniques and a final consolidation in an oven as shown schematically in Figure 1a. The electrode dimensions and position were selected to respect the requirements of having a CE larger than the WE and to facilitate the electrical connections. The preform is heated above its glass-transition temperature in a drawing tower and undergoes a continuous plastic deformation, which results in an extended length of fibers. The high viscosity of all of the materials at the drawing temperature enables the preservation of the architecture of the starting cross section down to the fiber level (Figure 1b).[42,43] Dozens of meters of fibers can potentially be processed in a single draw and subsequently cut into thousands of centimeter-long fiber sensors (Figure 1c). Furthermore, the final dimension of the fibers can be easily tuned by varying the drawing speed.

The surface properties of the carbon electrodes were improved through a simple activation procedure consisting of the partial dissolution of the insulating polycarbonate matrix using DMF, as shown in the context of carbon-doped PLA electrode.[44] SEM micrographs of the surface of the WE before and after the DMF treatment are shown in Figure 2a and reveal a significant increase in the surface roughness and amount of carbon black exposed at the surface.

The CV curves of a polished and DMF-treated fiber were recorded in PBS and 150 μM APAP (Figure 2b). The probe consists of a 5 cm long electrochemical fiber with typical cross-sectional dimensions of 0.6 × 1.2 mm^2 and a WE surface of 0.045 mm^2. The voltammetric profile before activation shows a poorly defined oxidation peak around 0.5 V and a minor reduction peak, indicating an almost electrochemically

https://doi.org/10.1021/acsami.1c11593
ACS Appl. Mater. Interfaces XXXX, XXX, XXX−XXX

irreversible process. In comparison, a 4-fold increase in oxidation peak current is obtained after the chemical treatment due to the increase in the electroactive surface area. In addition, both the oxidation and reduction peaks are better defined at ∼0.4 and 0.1 V, respectively, which suggests better reversibility.

The influence of the scan rate (5−200 mV/s) on the CV profiles of a DMF-treated electrode was also examined in a 100 μM APAP solution (Figure 2c). The peak current appears to increase linearly with the square root of the scan rate (Figure 2c inset) for both the bare and DMF-treated electrodes, which indicates a diffusion-controlled system. Slopes of 7.7×10^{-4} and 5.9×10^{-3} A/(mV/s)$^{0.5}$ were measured for the bare and DMF-treated electrodes, respectively, which can be related to an increase in active surface area of 7.7 using the Randles−Sevčik equation. Furthermore, the separation between the anodic and cathodic peaks at lower scan rates is ∼150 mV (Figure S2), which suggests slow electron-transfer kinetics, and/or electrochemically irreversible conditions. Based on the relationship between the scan rate and peak-to-peak separation, the heterogeneous electron-transfer (HET) rate constant (k_0) for the activated electrode was calculated. An average value of 5.9×10^{-4} cm/s is obtained, which compares favorably with 3D-printed graphene electrode[39] and DMF-treated graphene/PLA electrodes[45] and confirms the successful activation of our electrodes.

We then characterize the voltammetric response to paracetamol (APAP) of our fiber tip sensor by scanning the potential from −0.6 to 1.3 V. Figure 3a shows an example of cyclic voltammogram with increasing APAP content from 50 to 300 μM. A linear increase in peak current with APAP concentration is observed in the tested range (Figure 3a, right). The sensitivity s of the sensor, defined as the slope of the fitting curve, is 0.37 nA/μM. This value is lower than values acquired with SPE electrodes in terms of absolute value, but compares favorably with values acquired with the commercial SPE if accounting for the different surface areas: 8×10^{-6} nA/μMμm^2 for the fiber tip, 4×10^{-6} nA/μMμm^2 for the SPE.[46] The limit of detection (LOD) is estimated by $3\sigma_{PBS}/s$, where σ_{PBS} is the standard deviation of measurements acquired with PBS only (n = 3) around the peak potential. The calculated value is 1.7 μM, which is also comparable to those usually acquired with SPE electrodes.[47] Finally, the repeatability of the fiber tip is excellent as shown by the very small standard deviation calculated after five sequences of measurements with the same fiber (Figure 3a).

We then demonstrate the potential of our device for continuous therapeutic drug monitoring (TDM) using chronoamperometry. TDM is a growing field of pharmaceutical research that aims at precisely measuring and controlling drug dosage in patient's biofluid to fit the therapeutic demand. As an example, APAP is one of the most used analgesic and antipyretic drug to moderate pain and reduce fever. Its usage in therapeutic doses is considered safe; however, overdoses can lead to liver, kidney, and renal damages. In the perspective of implantable sensors for in situ TDM, the possibility to reach extremely small electrode dimensions and precise arrangement with the proposed fiber geometry is a compelling advantage toward minimal footprints, high spatial and temporal resolution, and robustness.

The CA profile was obtained by applying a constant voltage of 500 mV and measuring the current over time while injecting APAP. Figure 3b shows a chronoamperometry with successive

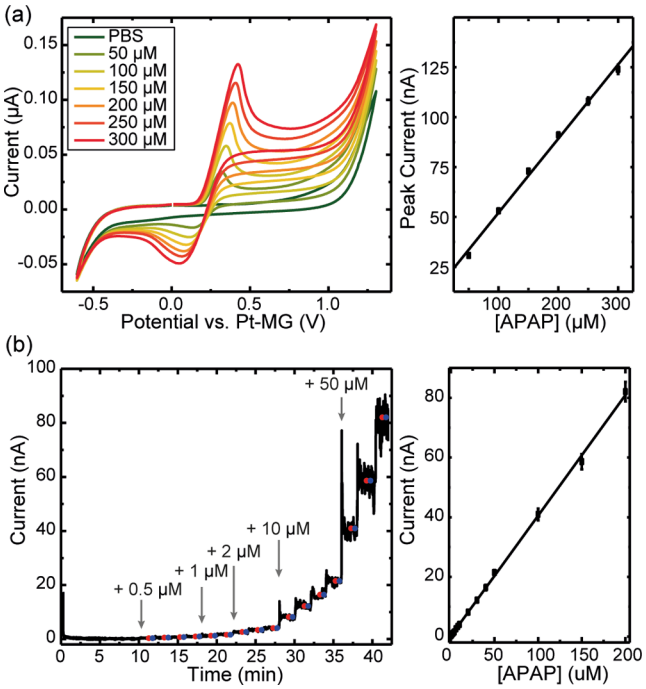


Figure 3. Characterization of the fiber tip electrochemical sensor for the detection of paracetamol. (a) Left: cyclic voltammograms of the fiber tip sensor with increasing concentrations of paracetamol (50−300 μM) in PBS. Right: calibration curve determined by measuring the peak oxidation current at each paracetamol concentration. The error bars represent the standard deviation of five consecutive measurements with the same fiber sensor. (b) Left: chronoamperometric response with successive injection of 0.5, 1, 2, 10, and 50 μM APAP at a stirring speed of 100 rpm. Right: calibration curve calculated by averaging the current over 30 s after each APAP injection as shown by the red and blue dots.

injections of 0.5, 1, 2, 10, and 50 μM APAP, under a constant stirring of 100 rpm. The calibration plot is calculated by averaging the current over 30 s after each APAP injection as shown by the red and blue dots in the CA profile. An excellent linear relationship (R^2 = 0.999) is observed in the tested range with a sensitivity of 0.40 nA/μM and an estimated LOD of 1.13 μM ($3\sigma_{PBS}/s$). The latter reveal the very good sensing performance of our fiber but need to be considered with caution since the values depend strongly on the experimental conditions such as the stirring rate, which influences the analyte diffusion at the sensor surface.

We now take advantage of the versatility of the thermal drawing process to elaborate a new type of high-aspect-ratio electrochemical cells. In this configuration, electrodes are exposed along the entire length of a hollow fiber, therefore combining a high electroactive area with microfluidics functionalities (Figure 4a). The probes are prepared by connecting one fiber end to a pipet tip, which allows us to draw a precise volume of solution into the fibers using a micropipette as shown in Figure 4b. The probe volume determines the length and surface area of the WE electrode and therefore the performance of the sensor. In a typical configuration, the probe consists of a 7 cm long electrochemical capillary cell with an outer cross section ranging between 0.85×1.40 and 1.6×2.6 mm^2. The CV response to APAP concentrations ranging from 10 to 300 μM, with a probe volume of 20 μL corresponding to a WE surface of 7.8 mm^2 (without surface activation), is presented in Figure 4c. A

https://doi.org/10.1021/acsami.1c11593
ACS Appl. Mater. Interfaces XXXX, XXX, XXX−XXX

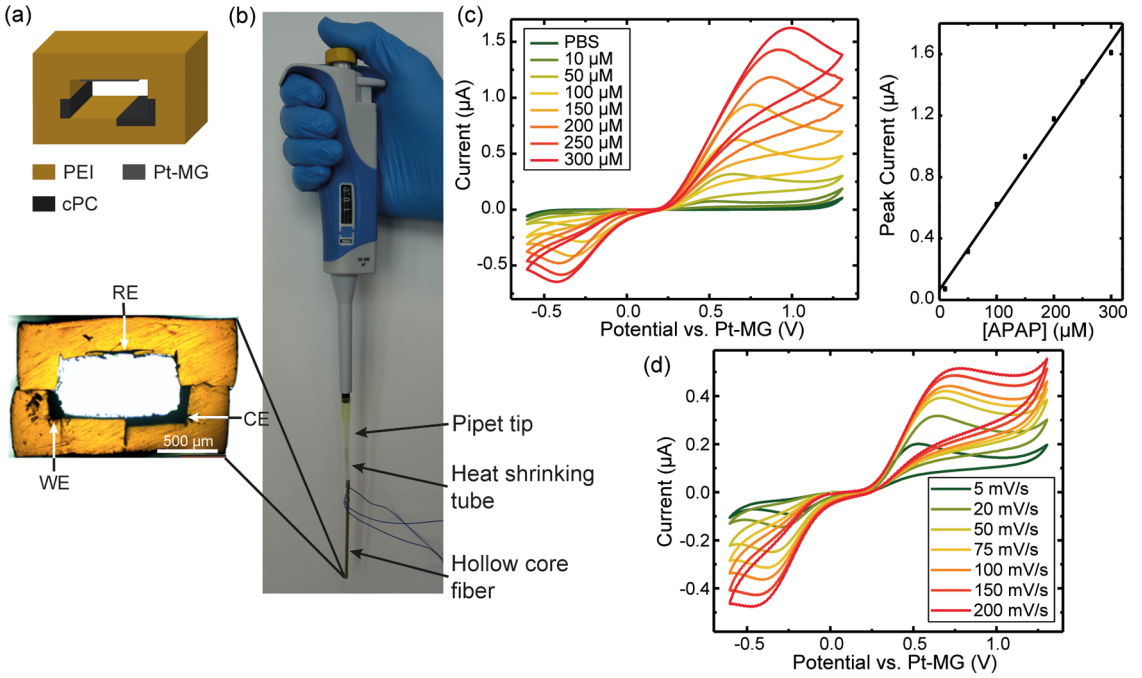


Figure 4. Pipet tip electrochemical sensor based on a capillary fiber. (a) Schematic and optical micrograph of the hollow core fiber cross section. (b) Schematic of the device, which comprises a hollow core electrochemical fiber, adapted to a pipet tip via heat-shrink tubing. The pipet enables precise drawing of the solution into the tip, while the high surface area of the electrochemical capillary maximizes the oxidation and reduction currents. (c) Cyclic voltammograms and calibration curve of the device (using Autolab) for APAP concentrations between 10 and 300 μM. (d) Cyclic voltammograms of the device in 50 μM APAP with increasing scan rate from 5 to 200 mV/s.

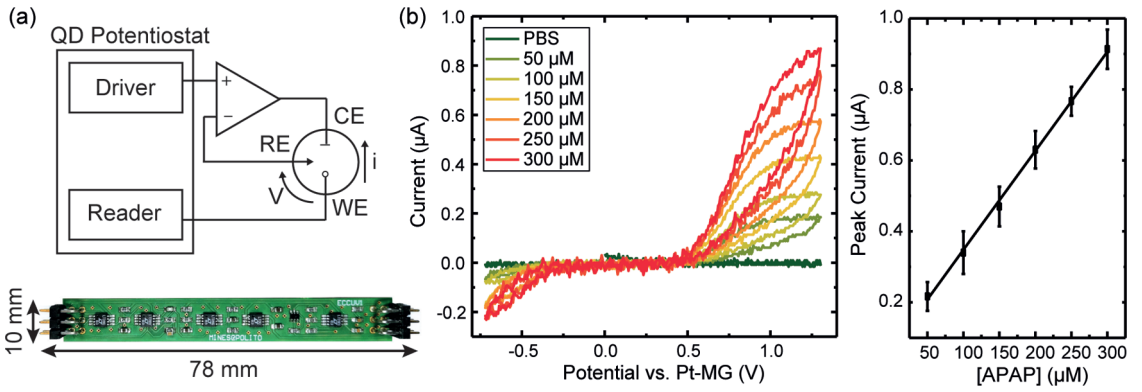


Figure 5. Demonstration of a fully portable electrochemical sensor system. (a) Schematic and photograph of the portable electronic system. (b) Cyclic voltammograms and calibration curve of a hollow core sensor using the portable system for APAP concentrations between 50 and 300 μM. The error bars represent the standard variation of three consecutive measurements.

sensitivity of 5.38 nA/μM and LOD of 0.58 μM can be deduced from the calibration curve (Figure 4c, right). A higher sensitivity is obtained compared to the fiber tip due to the larger WE surface area. However, the sensitivity per surface area is limited to 0.69×10^{-6} nA/μMμm^2 due to the lower amount of exposed carbon black and the slower scan rate. The LOD is comparable again to nonmodified SPE, which demonstrates the attractive performance of this fiber design enabling the analysis of small sample solutions.[47]

It is noteworthy that this capillary-based geometry induces a larger peak-to-peak distance, a stronger shift in peak voltage with increasing APAP concentration and wider peaks. Furthermore, the scan rate study showed ΔE_p larger than 600 mV even at scan rates as low as 5 mV/s (Figure 4d). Several factors related to the high-resistivity electrode material and sensor geometry can explain these differences. First, the electron-transfer rate is relatively slow when using bare cPC as opposed to its DMF-treated counterpart. Second, depending on the cell geometry, a significant ohmic drop that has to be subtracted from the applied potential can occur with low-conductivity electrolytes and high-resistance WE electrodes.[48,49] Finally, a specificity of our second cell architecture lies on the extended length of the WE in contact with the solution. Due to the high resistance of the WE (~MΩ), a large gradient of potential along the WE may be present and the redox reaction in portions of the electrode far from the electrical contact might be delayed to larger applied potential as demonstrated by simulation by Keil.[50] The two last effects are enhanced by large currents and therefore can explain the observed increase in peak-to-peak separation with increasing analyte concentration as well as the broadening of the peaks compared to the fiber tip geometry. Additional tests with a

https://doi.org/10.1021/acsami.1c11593
ACS Appl. Mater. Interfaces XXXX, XXX, XXX−XXX

fiber of smaller diameter showed larger ΔE_p, larger peak shift with concentration, and a strong broadening of the peaks, which support these different assumptions (Figures S3 and S4). Some modifications in the cell design could minimize these effects such as reducing the distance between the electrodes or adding a highly conductive metallic electrode behind the WE to reduce the gradient of potential along the fiber length, and will be the work of future studies.

Finally, the novel design of our probe sensor makes them attractive for point-of-care and in situ continuous monitoring in medical diagnostics. Such applications require a fully portable electronic device including a miniaturized potentiostat. Therefore, we connected our fiber sensor to a previously developed system.[47] The portable device is shown in Figure 5a and it consists of a custom 78 mm × 10 mm size printed circuit board (PCB) developed with commercial off-the-shelf (COTS) components, which implements a quasi-digital (QD) low-power potentiostat. The PCB relies on quasi-digital to analog conversion, and vice versa to reduce both size and power consumption.[47] The system consumes 19.5 mW in total. The CV curves acquired with the portable system connected to the hollow fiber probe are depicted in Figure 5b. The lower complexity of the system reduces its noise rejection (w.r.t. a lab instrument), yet the higher noise level does not prevent a very good level of sensitivity to APAP. The calibration curve shows high linearity (R^2 = 0.998), a sensitivity of 2.8 nA/μM, and an LOD of 11.3 μM, demonstrating the capabilities of our portable and small system to detect and measure APAP concentration in its therapeutic range (50:300 μM) with a suitable LOD (one-fifth of the minimum value of interest). Linearity and LOD may be improved by adding hardware or software filters, at the cost of an increase in power consumption and size.

CONCLUSIONS

In this article, we demonstrated a novel approach to produce all-in-fiber electrochemical sensors based on the thermal drawing approach. By leveraging recent advances in the multimaterial toolbox, in particular in the field of metallic glass processing, we monolithically integrated electroactive as well as inert pseudoreference electrodes into a three-electrode electrochemical cell assembly. The versatility of our approach for high-throughput production of compact electrochemical sensors was demonstrated in two innovative configurations, namely, a fiber tip microelectrode and a high-surface-area electrochemical capillary cell. We characterized the performances of our devices using paracetamol as a model analyte for personalized medicine, showing comparable sensitivity to commercial screen-printed electrodes. However, peak broadening and the absence of any surface functionalization may limit the selectivity of the device and should be investigated in more detail.

Future research direction should address the limitations of high resistance of the polymer composite through the addition of embedded highly conductive metal electrodes. In parallel, other materials compatible with the thermal drawing process could be investigated, such as carbon nanotubes dispersed in a polymer matrix or in addition to carbon black-filled polymers to improve the surface area and electrical conductivity of the composite electrode. The electrocatalytic activity of the platinum-based metallic glass toward hydrogen peroxide could also open up interesting perspectives for the detection of metabolites, such as enzyme-mediated glucose detection, or the monitoring of free radicals and antioxidants, a growing interest in food, environmental, and health monitoring.

Finally, minimizing further the dimensions of fiber-based electrochemical sensors could open their intraoperative use to guide medical interventions. With the ability to integrate additional functionalities such as microfluidics or optics unique to the multimaterial fiber platform, electrochemical methods could be applied for in situ detection of tumor-secreted biomarkers to then decide the release of chemotherapeutic drugs directly from the fiber into the tumor. In this field, electrochemical tissue oxygenation measurements could also enable a better targeting of, for example, hypoxic tumors, which are more resistant to radio and chemotherapy, paving the way toward new diagnosis and therapeutic tools.

ASSOCIATED CONTENT

Supporting Information

The Supporting Information is available free of charge at https://pubs.acs.org/doi/10.1021/acsami.1c11593.

Open-circuit potential, fiber tip: scan rate study, hollow core fiber: CV for various fiber dimensions and scan rate study (Figures S1−S4) (PDF)

AUTHOR INFORMATION

Corresponding Author

F. Sorin − *Institute of Materials, École Polytechnique Fédérale de Lausanne, 1015 Lausanne, Switzerland;* orcid.org/0000-0003-1019-6484; Email: fabien.sorin@epfl.ch

Authors

I. Richard − *Institute of Materials, École Polytechnique Fédérale de Lausanne, 1015 Lausanne, Switzerland;* orcid.org/0000-0001-7918-1913

B. Schyrr − *Institute of Materials, École Polytechnique Fédérale de Lausanne, 1015 Lausanne, Switzerland*

S. Aiassa − *Integrated Systems Laboratory, École Polytechnique Fédérale de Lausanne, 1015 Lausanne, Switzerland; Department of Electronics and Telecommunications, Politecnico di Torino, 10129 Turin, Italy*

S. Carrara − *Integrated Systems Laboratory, École Polytechnique Fédérale de Lausanne, 1015 Lausanne, Switzerland*

Complete contact information is available at: https://pubs.acs.org/10.1021/acsami.1c11593

Author Contributions

I.R. and B.S. contributed equally. The manuscript was written through contributions of all authors. All authors have given approval to the final version of the manuscript.

Notes

The authors declare no competing financial interest.

ACKNOWLEDGMENTS

F.S. acknowledges financial support by Swiss National Science Foundation (NSF, CH) (Grant No. 2000021_146871). F.S. also thanks the PHRT funding scheme (Grant No. 2018-532, "Spatially Resolved, Integrated Lab-On-Fiber Fluorescence Sensor for the Monitoring of Chronic and Acute Wounds") and the Competence Center for Materials Science and Technology (CCMX) Challenge financing scheme. The authors also thank Dr. Kurtuldu from the Laboratory of

Metal Physics and Technology (ETH Zürich) for the processing of the MG ribbons.

REFERENCES

(1) Arduini, F.; Micheli, L.; Moscone, D.; Palleschi, G.; Piermarini, S.; Ricci, F.; Volpe, G. Electrochemical Biosensors Based on Nanomodified Screen-Printed Electrodes: Recent Applications in Clinical Analysis. *TrAC, Trends Anal. Chem.* **2016**, *79*, 114−126.
(2) Li, M.; Li, D.-W.; Xiu, G.; Long, Y.-T. Applications of Screen-Printed Electrodes in Current Environmental Analysis. *Curr. Opin. Electrochem.* **2017**, *3*, 137−143.
(3) Muhammad, A.; Hajian, R.; Yusof, N. A.; Shams, N.; Abdullah, J.; Woi, P. M.; Garmestani, H. A Screen Printed Carbon Electrode Modified with Carbon Nanotubes and Gold Nanoparticles as a Sensitive Electrochemical Sensor for Determination of Thiamphenicol Residue in Milk. *RSC Adv.* **2018**, *8*, 2714−2722.
(4) Fanjulbolado, P.; Queipo, P.; Lamasardisana, P.; Costagarcia, A. Manufacture and Evaluation of Carbon Nanotube Modified Screen-Printed Electrodes as Electrochemical Tools. *Talanta* **2007**, *74*, 427−433.
(5) Arduini, F.; Di Nardo, F.; Amine, A.; Micheli, L.; Palleschi, G.; Moscone, D. Carbon Black-Modified Screen-Printed Electrodes as Electroanalytical Tools. *Electroanalysis* **2012**, *24*, 743−751.
(6) Randviir, E. P.; Brownson, D. A. C.; Metters, J. P.; Kadara, R. O.; Banks, C. E. The Fabrication, Characterisation and Electrochemical Investigation of Screen-Printed Graphene Electrodes. *Phys. Chem. Chem. Phys.* **2014**, *16*, 4598.
(7) Xie, X.; Stueben, D.; Berner, Z. The Application of Micro-electrodes for the Measurements of Trace Metals in Water. *Anal. Lett.* **2005**, *38*, 2281−2300.
(8) Stanley, J.; Pourmand, N. Nanopipettes—The Past and the Present. *APL Mater.* **2020**, *8*, No. 100902.
(9) Umehara, S.; Karhanek, M.; Davis, R. W.; Pourmand, N. Label-Free Biosensing with Functionalized Nanopipette Probes. *Proc. Natl. Acad. Sci. U.S.A.* **2009**, *106*, 4611−4616.
(10) Vafaye, S. E.; Rahman, A.; Safaeian, S.; Adabi, M. An Electrochemical Aptasensor Based on Electrospun Carbon Nanofiber Mat and Gold Nanoparticles for the Sensitive Detection of Penicillin in Milk. *J. Food Meas. Charact.* **2021**, *15*, 876−882.
(11) Adabi, M.; Adabi, M. Electrodeposition of Nickel on Electrospun Carbon Nanofiber Mat Electrode for Electrochemical Sensing of Glucose. *J. Dispersion Sci. Technol.* **2021**, *42*, 262−269.
(12) Katseli, V.; Economou, A.; Kokkinos, C. Single-Step Fabrication of an Integrated 3D-Printed Device for Electrochemical Sensing Applications. *Electrochem. Commun.* **2019**, *103*, 100−103.
(13) Cardoso, R. M.; Kalinke, C.; Rocha, R. G.; dos Santos, P. L.; Rocha, D. P.; Oliveira, P. R.; Janegitz, B. C.; Bonacin, J. A.; Richter, E. M.; Munoz, R. A. A. Additive-Manufactured (3D-Printed) Electrochemical Sensors: A Critical Review. *Anal. Chim. Acta* **2020**, *1118*, 73−91.
(14) Honeychurch, K. C.; Rymansaib, Z.; Iravani, P. Anodic Stripping Voltammetric Determination of Zinc at a 3-D Printed Carbon Nanofiber−Graphite−Polystyrene Electrode Using a Carbon Pseudo-Reference Electrode. *Sens. Actuators, B* **2018**, *267*, 476−482.
(15) Glavan, A. C.; Christodouleas, D. C.; Mosadegh, B.; Yu, H. D.; Smith, B. S.; Lessing, J.; Fernández-Abedul, M. T.; Whitesides, G. M. Folding Analytical Devices for Electrochemical ELISA in Hydrophobic RH Paper. *Anal. Chem.* **2014**, *86*, 11999−12007.
(16) Ambrosi, A.; Pumera, M. 3D-Printing Technologies for Electrochemical Applications. *Chem. Soc. Rev.* **2016**, *45*, 2740−2755.
(17) Liyarita, B. R.; Ambrosi, A.; Pumera, M. 3D-Printed Electrodes for Sensing of Biologically Active Molecules. *Electroanalysis* **2018**, *30*, 1319−1326.
(18) Hamzah, H. H.; Shafiee, S. A.; Abdalla, A.; Patel, B. A. 3D Printable Conductive Materials for the Fabrication of Electrochemical Sensors: A Mini Review. *Electrochem. Commun.* **2018**, *96*, 27−31.
(19) Yan, W.; Page, A.; Nguyen, D.; Qu, Y.; Sordo, F.; Wei, L.; Sorin, F. Advanced Multimaterial Electronic and Optoelectronic Fibers and Textiles. *Adv. Mater.* **2019**, *31*, No. 1802348.
(20) Bayindir, M.; Abouraddy, A. F.; Sorin, F.; Joannopoulos, J. D.; Fink, Y. Detectors. *Opt. Photonics News* **2004**, *15*, 24.
(21) Leber, A.; Page, A. G.; Yan, D.; Qu, Y.; Shadman, S.; Reis, P.; Sorin, F. Compressible and Electrically Conducting Fibers for Large-Area Sensing of Pressures. *Adv. Funct. Mater.* **2020**, *30*, No. 1904274.
(22) Qu, Y.; Nguyen-Dang, T.; Page, A. G.; Yan, W.; Das Gupta, T.; Rotaru, G. M.; Rossi, R. M.; Favrod, V. D.; Bartolomei, N.; Sorin, F. Superelastic Multimaterial Electronic and Photonic Fibers and Devices via Thermal Drawing. *Adv. Mater.* **2018**, *30*, No. 1707251.
(23) Leber, A.; Dong, C.; Chandran, R.; Das Gupta, T.; Bartolomei, N.; Sorin, F. Soft and Stretchable Liquid Metal Transmission Lines as Distributed Probes of Multimodal Deformations. *Nat. Electron.* **2020**, *3*, 316−326.
(24) Dong, C.; Leber, A.; Das Gupta, T.; Chandran, R.; Volpi, M.; Qu, Y.; Nguyen-Dang, T.; Bartolomei, N.; Yan, W.; Sorin, F. High-Efficiency Super-Elastic Liquid Metal Based Triboelectric Fibers and Textiles. *Nat. Commun.* **2020**, *11*, No. 3537.
(25) Yan, W.; Richard, I.; Kurtuldu, G.; James, N. D.; Schiavone, G.; Squair, J. W.; Nguyen-Dang, T.; Das Gupta, T.; Qu, Y.; Cao, J. D.; Ignatans, R.; Lacour, S. P.; Tileli, V.; Courtine, G.; Löffler, J. F.; Sorin, F. Structured Nanoscale Metallic Glass Fibres with Extreme Aspect Ratios. *Nat. Nanotechnol.* **2020**, *15*, 875−882.
(26) Guo, Y.; Jiang, S.; Grena, B. J. B.; Kimbrough, I. F.; Thompson, E. G.; Fink, Y.; Sontheimer, H.; Yoshinobu, T.; Jia, X. Polymer Composite with Carbon Nanofibers Aligned during Thermal Drawing as a Microelectrode for Chronic Neural Interfaces. *ACS Nano* **2017**, *11*, 6574−6585.
(27) Carvalho, R. C.; Mandil, A.; Prathish, K. P.; Amine, A.; Brett, C. M. A. Carbon Nanotube, Carbon Black and Copper Nanoparticle Modified Screen Printed Electrodes for Amino Acid Determination. *Electroanalysis* **2013**, *25*, 903−913.
(28) Vicentini, F. C.; Ravanini, A. E.; Figueiredo-Filho, L. C. S.; Iniesta, J.; Banks, C. E.; Fatibello-Filho, O. Imparting Improvements in Electrochemical Sensors: Evaluation of Different Carbon Blacks That Give Rise to Significant Improvement in the Performance of Electroanalytical Sensing Platforms. *Electrochim. Acta* **2015**, *157*, 125−133.
(29) Nguyen-Dang, T.; Page, A. G.; Qu, Y.; Volpi, M.; Yan, W.; Sorin, F. Multi-Material Micro-Electromechanical Fibers with Bendable Functional Domains. *J. Phys. D: Appl. Phys.* **2017**, *50*, No. 144001.
(30) Qin, F.; Bae, G. T.; Dan, Z.; Lee, H.; Kim, N. J. Corrosion Behavior of the Mg65CU25Gd10 Bulk Amorphous Alloys. *Mater. Sci. Eng. A* **2007**, *449−451*, 636−639.
(31) Kawashima, A.; Ohmura, K.; Yokoyama, Y.; Inoue, A. The Corrosion Behaviour of Zr-Based Bulk Metallic Glasses in 0.5M NaCl Solution. *Corros. Sci.* **2011**, *53*, 2778−2784.
(32) Kou, H.; Li, Y.; Zhang, T.; Li, J.; Li, J. Electrochemical Corrosion Properties of Zr- and Ti-Based Bulk Metallic Glasses. *Trans. Nonferrous Met. Soc. China* **2011**, *21*, 552−557.
(33) Schroers, J.; Johnson, W. L. Highly Processable Bulk Metallic Glass-Forming Alloys in the Pt−Co−Ni−Cu−P System. *Appl. Phys. Lett.* **2004**, *84*, 3666−3668.
(34) Sekol, R. C.; Kumar, G.; Carmo, M.; Gittleson, F.; Hardesty-Dyck, N.; Mukherjee, S.; Schroers, J.; Taylor, A. D. Bulk Metallic Glass Micro Fuel Cell. *Small* **2013**, *9*, 2081−2085.
(35) Carmo, M.; Sekol, R. C.; Ding, S.; Kumar, G.; Schroers, J.; Taylor, A. D. Bulk Metallic Glass Nanowire Architecture for Electrochemical Applications. *ACS Nano* **2011**, *5*, 2979−2983.
(36) Doubek, G.; Sekol, R. C.; Li, J.; Ryu, W.-H.; Gittleson, F. S.; Nejati, S.; Moy, E.; Reid, C.; Carmo, M.; Linardi, M.; Bordeenithikasem, P.; Kinser, E.; Liu, Y.; Tong, X.; Osuji, C. O.; Schroers, J.; Mukherjee, S.; Taylor, A. D. Guided Evolution of Bulk Metallic Glass Nanostructures: A Platform for Designing 3D Electrocatalytic Surfaces. *Adv. Mater.* **2016**, *28*, 1940−1949.
(37) Schroers, J.; Kumar, G.; Hodges, T. M.; Chan, S.; Kyriakides, T. R. Bulk Metallic Glasses for Biomedical Applications. *JOM* **2009**, *61*, 21−29.

https://doi.org/10.1021/acsami.1c11593
ACS Appl. Mater. Interfaces XXXX, XXX, XXX−XXX

(38) Klingler, R. J.; Kochi, J. K. Electron-Transfer Kinetics from Cyclic Voltammetry. Quantitative Description of Electrochemical Reversibility. *J. Phys. Chem. A* **1981**, *85*, 1731−1741.
(39) Katic, V.; dos Santos, P. L.; dos Santos, M. F.; Pires, B. M.; Loureiro, H. C.; Lima, A. P.; Queiroz, J. C. M.; Landers, R.; Muñoz, R. A. A.; Bonacin, J. A. 3D Printed Graphene Electrodes Modified with Prussian Blue: Emerging Electrochemical Sensing Platform for Peroxide Detection. *ACS Appl. Mater. Interfaces* **2019**, *11*, 35068−35078.
(40) Ribeiro, A. C. F.; Barros, M. C. F.; Veríssimo, L. M. P.; Santos, C. I. A. V.; Cabral, A. M. T. D. P. V.; Gaspar, G. D.; Esteso, M. A. Diffusion Coefficients of Paracetamol in Aqueous Solutions. *J. Chem. Thermodyn.* **2012**, *54*, 97−99.
(41) Lounasvuori, M. M.; Kelly, D.; Foord, J. S. Carbon Black as Low-Cost Alternative for Electrochemical Sensing of Phenolic Compounds. *Carbon* **2018**, *129*, 252−257.
(42) Nguyen Dang, T.; Richard, I.; Goy, E.; Sordo, F.; Sorin, F. Insights into the Fabrication of Sub-100 Nm Textured Thermally Drawn Fibers. *J. Appl. Phys.* **2019**, *125*, No. 175301.
(43) Nguyen-Dang, T.; de Luca, A. C.; Yan, W.; Qu, Y.; Page, A. G.; Volpi, M.; Das Gupta, T.; Lacour, S. P.; Sorin, F. Controlled Sub-Micrometer Hierarchical Textures Engineered in Polymeric Fibers and Microchannels via Thermal Drawing. *Adv. Funct. Mater.* **2017**, *27*, No. 1605935.
(44) Manzanares Palenzuela, C. L.; Novotný, F.; Krupička, P.; Sofer, Z.; Pumera, M. 3D-Printed Graphene/Polylactic Acid Electrodes Promise High Sensitivity in Electroanalysis. *Anal. Chem.* **2018**, *90*, 5753−5757.
(45) Browne, M. P.; Novotný, F.; Sofer, Z.; Pumera, M. 3D Printed Graphene Electrodes' Electrochemical Activation. *ACS Appl. Mater. Interfaces* **2018**, *10*, 40294−40301.
(46) Aliakbarinodehi, N.; Stradolini, F.; Nakhjavani, S. A.; Tzouvadaki, I.; Taurino, I.; De Micheli, G.; Carrara, S. Performance of Carbon Nano-Scale Allotropes in Detecting Midazolam and Paracetamol in Undiluted Human Serum. *IEEE Sens. J.* **2018**, *18*, 5073−5081.
(47) Aiassa, S.; Stradolini, F.; Tuoheti, A.; Carrara, S.; Demarchi, D. In *Quasi-Digital Biosensor-Interface for a Portable Pen to Monitor Anaesthetics Delivery*, 15th Conference on Ph.D Research in Microelectronics and Electronics (PRIME), 2019.
(48) Myland, J. C.; Oldham, K. B. Uncompensated Resistance. 1. The Effect of Cell Geometry. *Anal. Chem.* **2000**, *72*, 3972−3980.
(49) Zhang, G.; Cuharuc, A. S.; Güell, A. G.; Unwin, P. R. Electrochemistry at Highly Oriented Pyrolytic Graphite (HOPG): Lower Limit for the Kinetics of Outer-Sphere Redox Processes and General Implications for Electron Transfer Models. *Phys. Chem. Chem. Phys.* **2015**, *17*, 11827−11838.
(50) Keil, R. G. Resistive Electrode Effects on Cyclic Voltammetry. *J. Electrochem. Soc.* **1986**, *133*, 1375.

https://doi.org/10.1021/acsami.1c11593
ACS Appl. Mater. Interfaces XXXX, XXX, XXX−XXX